Cubic-spline expansion for a two-dimensional periodic conductor in free space

Wei Chien, Chung-Hsin Huang and Chien-Ching Chiu
Electrical Engineering Department, Tamkang University, Tamsui, Taiwan
E-mail: chiu@ee.tku.edu.tw

Abstract. This paper presents a computational approach to the imaging of a two-dimensional periodic conductor. Both cubic-spline method and trigonometric series for shape description are used and compared. A periodic conducting cylinder with unknown shape in free space and the scattered field is recorded outside. Based on the boundary condition and the recorded scattered field, a set of nonlinear integral equations is derived and the imaging problem is reformulated into an optimization problem. The genetic algorithm is employed to find out the global extreme solution of the object function. It is found that the shape described by cubic-spline can be reconstructed. In such a case, Fourier series expansion will fail. Even when the initial guess is far away from the exact one, the cubic-spline expansion and genetic algorithm can avoid the local extreme and converge to a global extreme solution. Numerical results are given to show that the shape description by using cubic-spline method is much better than that by the Fourier series. In addition, the effect of Gaussian noise on the reconstruction is investigated.

1. Introduction

Due to large domain of applications such as non-destructive problem, geophysical prospecting and determination of underground tunnels and pipelines, etc, the inverse scattering problems related to the buried bodies has been important in the scattering theory. In the past 20 years, many rigorous methods have been developed to solve the exact equations [1–9]. However, inverse problems of this type are difficult to solve because they are illposed and nonlinear [10]. As a result, many inverse problems are reformulated into optimization ones and then numerically solved by different iterative methods such as the Newton-Kantorovitch method [1–5], the Levenberg-Marquardt algorithm [6–8], and the successive-overrelaxation method [9]. Most of these approaches employ the gradient-based searching scheme to find the extreme of the cost function, which are highly dependent on the initial guess and usually get trapped in the local extreme. The genetic algorithm [11] is an evolutionary algorithm that uses the stochastic mechanism to search through the parameter space. As compared to the gradient-based searching techniques, the genetic algorithm is less prone to converge to a local extreme. This renders it an ideal candidate for global optimization. Recently, researchers have applied GA together with electromagnetic solver to attack the inverse scattering problem mainly in two ways. One is surface reconstruction approach, the other is volume reconstruction approach. Chiu [12] first applied the GA for the inversion of a perfectly conducing cylinder with the geometry described by a Fourier series (surface reconstruction approach), while Takenaka [13], Meng [14] and Zhou [15] used the concept of local shape function to describe the conducting objects (volume reconstruction approach). Alternatively, Chien [16],
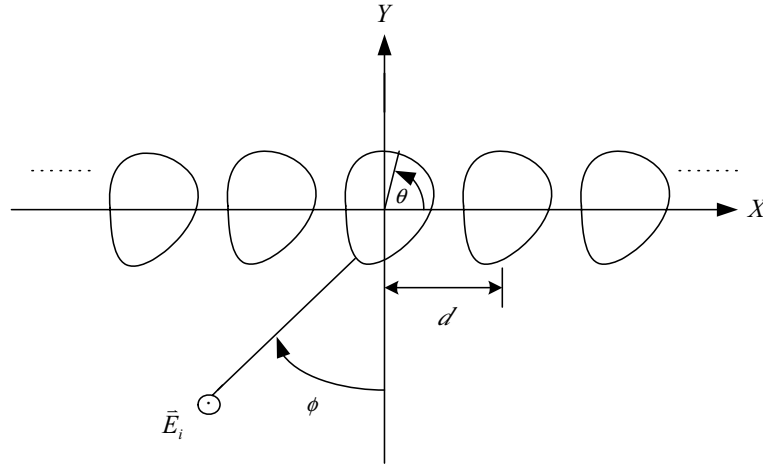
Fig. 1. Geometry of the problem in (x, y) plane.

Zhou [17] and Qing [18] used B-splines to describe the geometry of a perfect conducting cylinder. The 2-D perfectly conducting cylinders are denoted by local shape functions $\rho = F(\theta)$ with respect to their local origins which can be continuous or discrete. However, to the best of our knowledge, there are still no numerical results that discussed which shape description is more suitable in a two-dimensional periodic conducting cylinder inverse problem in free space. In this paper, we present a computational method based on the genetic algorithm to recover the shape of a two-dimensional periodic conducting cylinder in free space and test which shape description has more limitations in the inverse problem. In Section 2, the theoretical formulation for the electromagnetic imaging is presented. The general principle of the genetic algorithm and the way we applied them to the imaging problem are described. Numerical results for reconstructing objects of different shapes are given in Section 3. Finally, some conclusions are drawn in Section 4.

2. Theoretical formulation

A periodic two-dimensional metallic cylinder is situated in a background medium with a permittivity ε_o and a permeability μ_o, as shown in Fig. 1. The array is periodic in the x-direction with a periodic length d and is uniform in the z-direction. The cross section of the metallic cylinder is assumed to be described in polar coordinates in xy plane by the equation $\rho = F(\theta)$. A plane wave whose electric field vector is parallel to the z-axis (i.e., transverse magnetic, or TM, polarization) is incident upon the periodic cylinder. Let $\vec{E}_i$ denote the incident wave with incident angel ϕ, as shown in Fig. 1. The scattered field, $\vec{E}_s = E_s \hat{z}$ can be expressed by

$$E_s(x, y) = \int_0^{2\pi} G_i(x, y; x, y') J(\theta') d\theta' \tag{1}$$

where

$$G_i(x, y; x', y') = \sum_{l=-\infty}^{\infty} \frac{1}{2\alpha_l d} \exp(-\alpha_l |y - y'|) \exp(-jk_l(x - x')) \tag{2}$$

$$J(\theta) = -j\omega\mu_0 \sqrt{F^2(\theta) + F'^2(\theta)} J_s(\theta) \tag{3}$$

with

$$\alpha_l = \begin{cases} j\sqrt{k^2 - k_l^2} & , k^2 > k_l^2 \\ \sqrt{k_l^2 - k^2} & , k^2 \leqslant k_l^2 \end{cases}, k_l = \frac{2\pi l}{d} + k\sin\phi, k^2 = \omega^2\varepsilon_0\mu_0$$

Here $G_i(x, y; x', y')$ is the two–dimensional periodic Green's function [19,20], and $J_s(\theta)$ is the induced surface current density which is proportional to the normal derivative of electric field on the conductor surface. The boundary condition at the surface of the scatterer states that the total tangential electric field must be zero and this yield an integral equation for $J(\theta)$:

$$E_i(F(\theta), \theta) = -\int_0^{2\pi} G_i(x, y, x', y')J(\theta')d\theta' \tag{4}$$

For the direct scattering problem, the scattered field E_s is calculated by assuming that the periodic length d and the shape function $F(\theta)$ of the object is known. This can be achieved by first solving J(θ) in Eq. (4) and calculating E_s in Eq. (1). For numerical calculation of the direct problem, the contour is first divided into sufficient small segments so that the induced surface current can be considered constant over each segment. Then the moment method is used to solve Eq. (4) and Eq. (1) with pulse basis function for expanding and Dirac delta function for testing. Note that, for numerical implementation of the periodic Green's function, we might face some difficulties in calculating this function. In fact, when y approaches y', the infinite series in Eq. (3) is very poor convergent. Fortunately, the infinite series may be rewritten as a rapidly convergent series plus an asymptotic series which can be summed efficiently. Thus the infinite series in the periodic Green's function can be calculated efficiently [19,20].

Let us consider the following inverse problem: given the scattered electric field E_s measured outside the scatterer, determine the shape function $F(\theta)$ of the object. Two different shape expansions are considered as follows:

(A) Shape expansion by the Fourier series:

Assume the approximate center of the scatterer, which in fact can be any point inside the scatterer, is known. Then the shape function $F(\theta)$ can be expanded by the Fourier series as follows:

$$F(\theta) \cong \sum_{n=0}^{\frac{N}{2}} B_n \cos(n\theta) + \sum_{n=1}^{\frac{N}{2}} C_n \sin(n\theta) \tag{5}$$

where B_n and C_n are real coefficients to be determined and $(N + 1)$ is the terms to expand the shape.

(B) Shape expansion by the cubic-spline:

The geometry of the cubic-spline is shown in Fig. 2 [21,22]. First, the shape is divided with N segments and $N+1$ separated points. We denote the separated points by polarized-coordinate expression as (ρ_0, θ_0), $(\rho_1, \theta_1), \ldots, (\rho_N, \theta_N)$, where $0° \leqslant \theta_i \leqslant 360°$, $i = 0 \ldots$N, $\theta_0 = 0°$, $\theta_N = 360°$ and $\theta_0 < \theta_1 < \ldots < \theta_N$. ρ_i is the distance between the point (ρ_i, θ_i) and the center point (x_0, y_0). $p_i(\theta)$ is the function of cubic line which link the points $(\theta_{i-1}, \rho_{i-1})$ and (θ_i, ρ_i).

The discretization number of $J(\theta)$ for the inverse problem must be different from that for the direct problem. Since it is crucial that the synthetic data generated by a direct solver are not like those obtained by the inverse solver, the discretization number for the direct problem is twice of that for the inverse
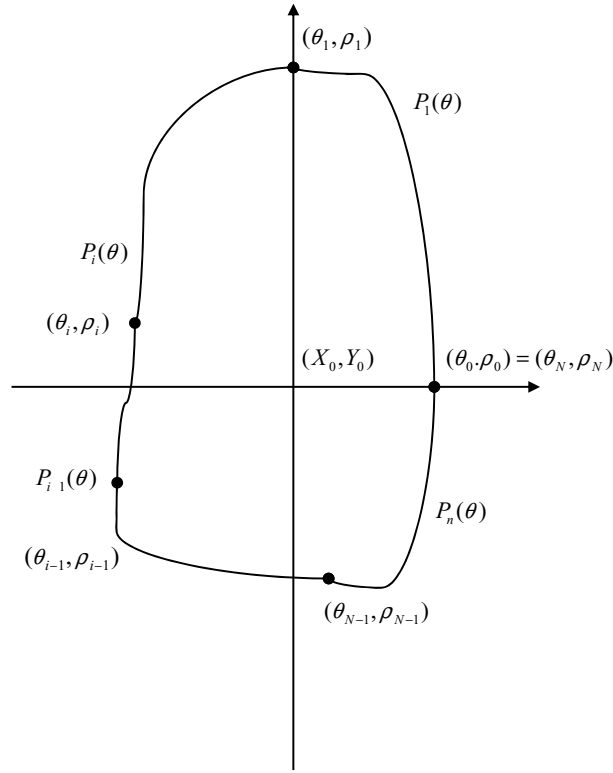
Fig. 2. Geometry of the cubic-spline. (θ_i, ρ_i) is the polarized-coordinate expression for each point and $p_i(\theta)$ is the function of the cubic line which links the points $(\theta_{i-1}, \rho_{i-1})$ and (θ_i, ρ_i).

problem in this study. For the inversion procedure, the genetic algorithm is employed to maximize the following object function:

$$SF = \left\{ \sum_{x=1}^{X_t} \left| E_s^{\exp}(\vec{r}_x) - E_s^{cal}(\vec{r}_x) \right|^2 \Bigg/ \sum_{x=1}^{X_t} \left| E_s^{\exp}(\vec{r}_x) \right|^2 + \beta \left| F'(\theta) \right|^2 \right\}^{-1/2} \tag{6}$$

where X_T is the total number of measurement points, and $E_s^{cal}(\vec{r})$ and $E_s^{\exp}(\vec{r})$ are the calculated scattered field and the measured scattered field, respectively. Note that there is a regularization term $\beta \left| F'(\theta) \right|^2$ added in Eq. (6). The added term $\beta \left| F'(\theta) \right|^2$ can, to a certain extent, be interpreted as the smoothness requirement for the shape function $F(\theta)$. Therefore, the maximization of SF can be interpreted as the minimization of the least-square error between the measured and the calculated fields with the constraint of smooth boundary. Typical values of β range from 0.00001 to 10. The optimal value of β depends mostly on the dimensions of the geometry. One can always choose a large enough value to ensure the convergence, although overestimation would result in a very smooth reconstructed image. Technically, we can let the value of β decrease gradually during the course of convergence [4].

Genetic algorithms are the global numerical optimization methods based on genetic recombination and evaluation in nature [20]. They use the iterative optimization procedures that start with a randomly selected population of potential solutions, and then gradually evolve toward a better solution through the application of the genetic operators. Genetic algorithms typically operate on a discretized and coded
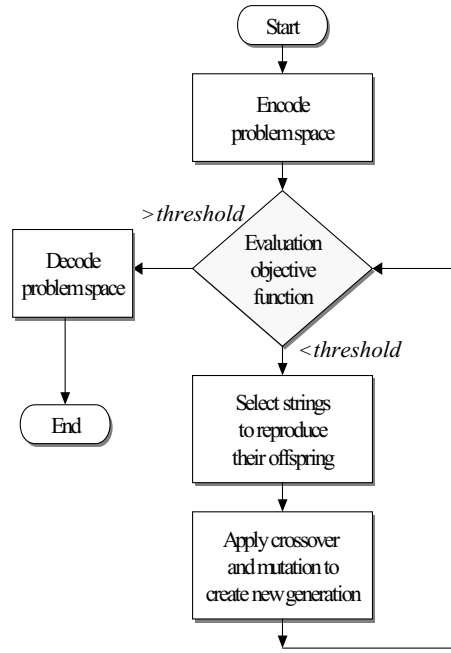
Fig. 3. Flowchart for the genetic algorithm.

representation of the parameters rather than on the parameters themselves. These representations are often considered to be "chromosomes," while the individual element that constitutes the chromosome is the "genes". Simple but often very effective chromosome representations for optimization problem involving several continuous parameters can be obtained through the juxtaposition of discretized binary representations of the individual parameters. In our problem, parameters ρ_i are given by the following equation:

$$\rho_i = p_{\min} + \frac{p_{\max} - p_{\min}}{2^L - 1} \sum_{j=0}^{L-1} b_j^{\rho_i} \tag{7}$$

$b_0^{\rho_i}, b_1^{\rho_i}, \ldots$ and $b_{L-1}^{\rho_i}$ (genes) are the L-bit string of the binary representation of ρ_i, and $p_{\min}$ and $p_{\max}$ are the minimum and the maximum values admissible for ρ_i, respectively. Here, $p_{\min}$ and $p_{\max}$ can be determined by prior knowledge of the object. Also, the finite resolution with ρ_i, can be tuned in practice is reflected in the number of bits assigned to it. The basic GA for which a flowchart is shown in Fig. 3 starts with a large population containing a total of X candidates. Each candidate is described by a chromosome. Then the initial population can simply be created by taking X random chromosomes. Finally, the GA iteratively generates a new population which is derived from the previous population through the application of the reproduction, crossover, and mutation operators.

3. Numerical results

We illustrate the performance of the proposed inversion algorithm and its sensitivity to random noise in the scattered field. Consider a perfectly conducting cylinder array with a periodic length d in free
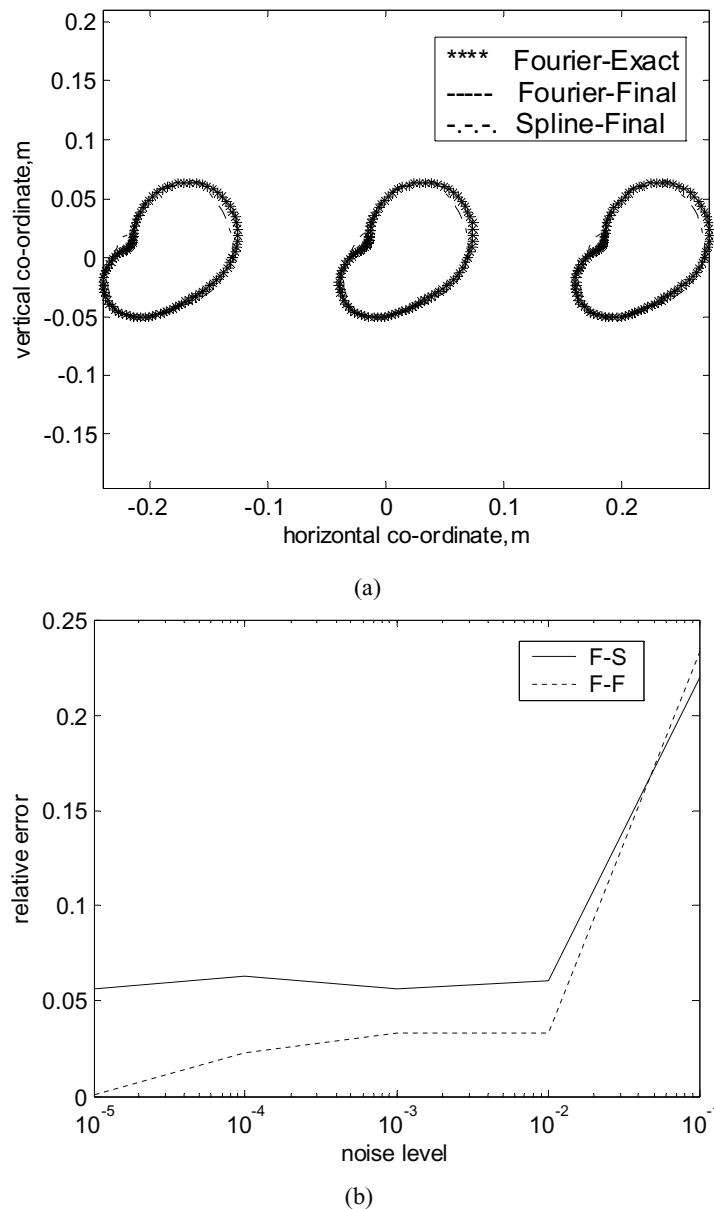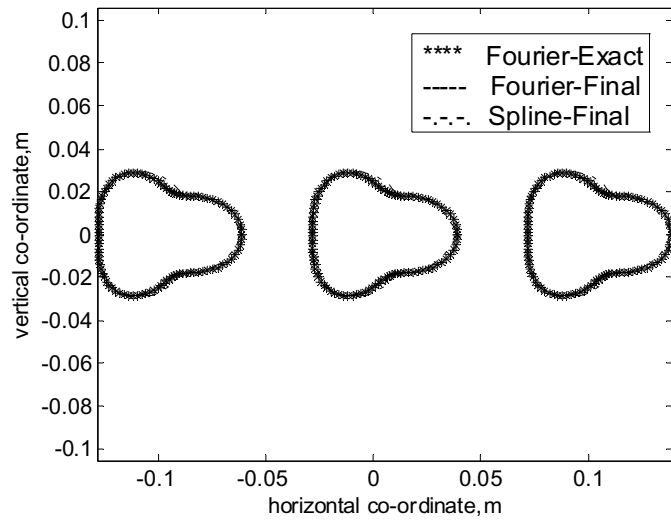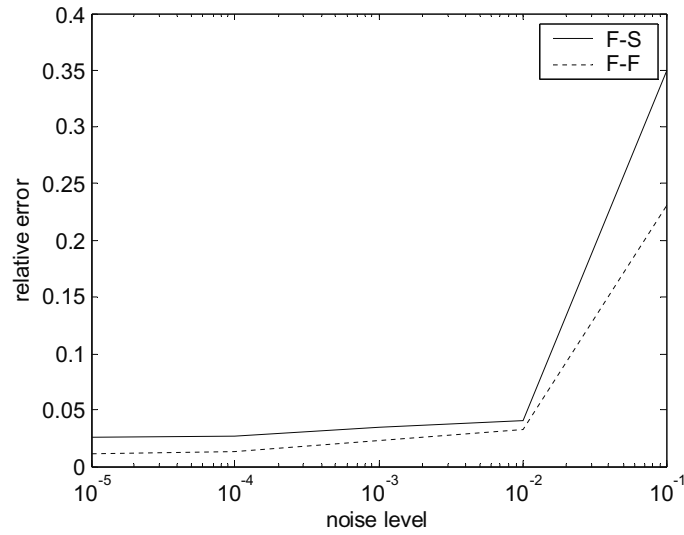
(a)

(b)

Fig. 4. (a) Shape function for example 1. The star curve represents the exact shape by Fourier-series, while the curve of long imaginary line is calculated shape by the Fourier-series and the curve of short imaginary line represents calculated shape by the cubic-spline in final result. (b) Shape function error as a function of noise levels for example 1 in each represented method. The F-S means that the shape function in direct problem is described by the Fourier-series and in inverse problem is described by the cubic-spline. The F-F means that the shape function both in direct and inverse problem are described by the Fourier-series.

space and a plane wave of unit amplitude is incident upon the object, as shown in Fig. 1. The frequency of the incident wave is chosen to be 3 GHz; i.e., the wavelength λ is 0.1 m. In the examples, the size of the scatterer is about one third of the wavelength, so the frequency is in the resonance range.

In our calculation, three examples are considered. To reconstruct the shape of the cylinder, the object is illuminated by two incident waves with incident angles $\phi = 45°$ and $135°$, and the measurement points

(a)

(b)

Fig. 5. (a) Shape function for example 2. The star curve represents the exact shape by Fourier-series, while the curve of long imaginary line is calculated shape by the Fourier-series and the curve of short imaginary line represents calculated shape by the cubic-spline in final result. (b) Shape function error as a function of noise levels for example 2 in each represented method. The F-S means that the shape function in direct problem is described by the Fourier-series and in inverse problem is described by the cubic-spline. The F-F means that the shape function both in direct and inverse problem are described by the Fourier-series.

are taken on two lines with $Y = \pm 2$ m from $x = -0.045$ to 0.045 m. Each line has nine measurement points. Note that for each incident angle eighteen measurement points at equal spacing are used, and there are totally 36 measurement points in each simulation. The population size is chosen as 250 (i.e., $M = 250$), upper than ten times of the number of unknowns by the experience of our simulations. The binary string length of the unknown coefficient, B_n (C_n or ρ_i), is set to be 16 bits (i.e., $L = 16$). The search range for the unknown coefficient of the shape function is chosen to be from 0 to 0.1. The extreme
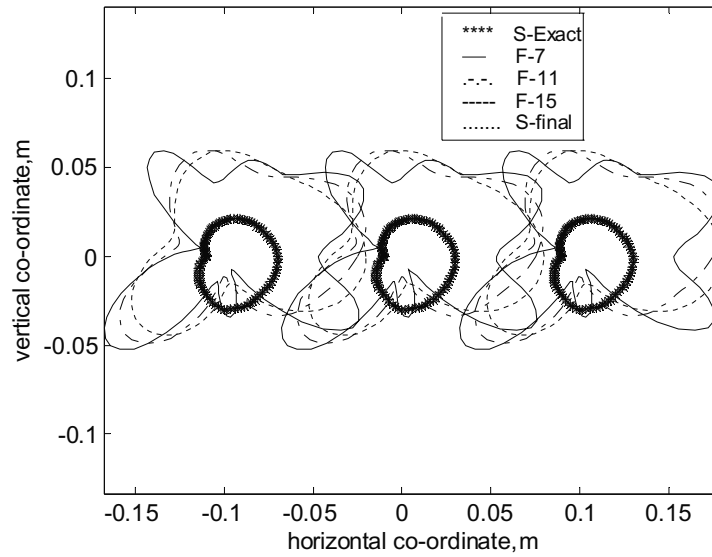
Fig. 6. Shape function for example 3. The star curve represents the exact shape by cubic-spline, while the curves of solid, short imaginary, long imaginary and dot lines are calculated shapes by the 7-terms, 11-terms, 15-terms Fourier-series and 8-point cubic-spline expands in final result.

value of the coefficient of the shape function can be determined by the prior knowledge of the objects. The crossover probability p_c and mutation probability p_m are set to be 0.8 and 0.04, respectively. The value of β is chosen to be 0.001. The maximum number of generation is set 1000. However, when the change of fitness value is less than 1% in 500 generations, the simulation will also stop.

In the first example, the shape function is given by $F(\theta) = (0.05 + 0.02\cos\theta + 0.015\sin 2\theta)$m with a periodic length $d = 0.2$ m and we use 7-unknown Fourier-series and 6-unknown cubic-spline expand to recover it. The reconstructed shape function for the best population member (chromosome) is plotted in Fig. 4(a). From Fig. 4(a), it is clear that reconstruction of the shape function is quite good for both Fourier-series and cubic-spline expand. To investigate the sensitivity of the imaging algorithm against random noise, two independent Gaussian noises with zero mean have been added to the real and imaginary parts of the simulated scattered fields. Normalized standard deviations of 10^{-5}, 10^{-4}, 10^{-3}, 10^{-2} and 10^{-1} are used in the simulations. The normalized standard deviation mentioned earlier is defined as the standard deviation of the Gaussian noise divided by the rms value of the scattered fields. Here, the signal-to-noise ratio (SNR) is inversely proportional to the normalized standard deviation. The relative error is defined as the root mean square error of $F(\theta)$. The numerical result for this example is plotted in Fig. 4(b).

In the second example, the shape function is selected to be $F(\theta) = (0.03 + 0.009\cos 3\theta)$m with a periodic length $d = 0.1$ m and we use 7-unknown Fourier-series and 6-unknown cubic-spline expand to recover it. Both Fourier-series and cubic-spline expand can recover it. Satisfactory results are shown in Fig. 5(a) and the relative error for different random noise level is shown in Fig. 5(b).

In the third example, the shape function is selected by the cubic-spline expand to be $\rho_0 = 0.03$ m, $\rho_1 = 0.02$ m, $\rho_2 = 0.01$ m and $\rho_3 = 0.03$ m with a periodic length $d = 0.1$ m, then we use 7-unknown, 11-unknown, 15-unknown Fourier-series expressions and 8-unknown cubic-spline expand to recover the shape. The results are shown in Fig. 6 and it is found that the Fourier-series can not recover the shape even the unknowns attained to 15.

4. Conclusions

An approach of shape description for a periodic metallic object in free space has been described in this paper. Based on the boundary condition and measured scattered field, we have derived a set of nonlinear integral equations and reformulated the imaging problem into an optimization problem. The genetic algorithm is then employed to find the microwave image of metallic cylinder. The contours of the cylinders described by cubic-spline expand or trigonometric series. Both shape functions are used in direct and inverse problems. In the base of Fourier series theorem, it needs infinite or a lot of terms to describe a shape. However, there are many limitations in the numerical experiments (eq. a huge number of unknown Fourier series terms in GA) and the characteristic of Fourier series expansion will cause a lot of unreasonable shapes in the inverse process (population produced by GA). On the contrary, the characteristic of cubic spline expansion will guarantee the shape description is reasonable and more variable than Fourier series expansion. Numerical results shown that we can not find the convergence solutions of random shapes by using a few terms of Fourier series expansion in the inverse problem, but the reconstructed results by cubic-spline expand is quite good. Using cubic-spline expand to solve the inverse problem seems more practicable than Fourier-series expression.

Acknowledgments

References

[1] A. Roger, Newton-Kantorovitch algorithm applied to an electromagnetic inverse problem, *IEEE Trans Antennas Propagat* **AP-29** (Mar. 1981), 232–238.

[2] C.C. Chiu and Y.W. Kiang, Inverse scattering of a buried conducting cylinder, *Inverse Problems* **7** (April 1991), 187–202.

[3] C.C. Chiu and Y.W. Kiang, Microwave imaging of multiple conducting cylinders, *IEEE Trans. Antennas Propagat* **40** (Aug. 1992), 933–941.

[4] G.P. Otto and W.C. Chew, Microwave inverse scattering-local shape function imaging for improved resolution of strong scatterers, *IEEE Trans Microwave Theory Tech* **42** (Jan. 1994), 137–142.

[5] R. Kress, A Newton method in inverse obstacle scattering Inverse Problem in Engineering Mechanics, H.D. Bui, et al. (Rotterdam: Balkema), 1994, 425–432.

[6] D. Colton and P. Monk, A novel method for solving the inverse scattering problem for time-harmonic acoustic waves in the resonance region II, *SIAM J Appl Math* **46** (June 1986), 506–523.

[7] A. Kirsch, R. Kress, P. Monk and A. Zinn, Two methods for solving the inverse acoustic scattering problem, *Inverse problems* **4** (Aug. 1998), 749–770.

[8] F. Hettlich, Two methods for solving an inverse conductive scattering problem, *Inverse Problems* **10** (1994), 375–385.

[9] R.E. Kleinman and P.M. van den Berg, Two-dimensional location and shape reconstruction, *Radio Sci* **29** (July-Aug. 1994), 1157–1169.

[10] T. Hohage, *Iterative Methods in Inverse Obstacle Scattering: Regularization Theory of Linear and Nonlinear Exponentially Ill-Posed Problems*, Dissertation Linz, 1999.

[11] D.E. Goldgreg, *Genetic Algorithm in Search*, Optimization and Machine Learning, Addison-Wesley, 1989.

[12] C.C. Chiu and P.T. Liu, Image reconstruction of a perfectly conducting cylinder by the genetic algorithm, *IEE Proc Micro Antennas Propagat* **143** (June 1996), 249–253.

[13] T. Takenaka, Z.Q. Meng, T. Tanaka and W.C. Chew, Local shape function combined with genetic algorithm applied to inverse scattering for strips, *Microwave and Optical Technology Letters* **16** (December 1997), 337–341.

[14] Z.Q. Meng, T. Takenaka and T. Tanaka, Image reconstruction of two-dimensional impenetrable objects using genetic algorithm, *Journal of Electromagnetic Waves and Applications* **13** (1999), 95–118.

[15] Y. Zhou and H. Ling, Electromagnetic inversion of Ipswich objects with the use of the genetic algorithm, *Microwave and Optical Technology Letters* **33** (June 2002), 457–459.

[16] W. Chien, *Using the Genetic Algorithm to Reconstruct the Two-Dimensional Conductor*, Master Thesis, National Tamkang University, Department of Electrical Engineering, June 1999.

[17] Y. Zhou, J. Li and H. Ling, Shape inversion of metallic cavities using hybrid genetic algorithm combined with tabu list, *Electronics Letters* **39** (Feb. 2003), 280–281.

[18] A. Qing, An experimental study on electromagnetic inverse scattering of a perfectly conducting cylinder by using the real-coded genetic algorithm, *Microwave and Optical Technology Letters* **30** (Sept. 2001), 315–320.

[19] G.S. Wallinga, E.J. Rothwell, K.M. Chen and D.P. Nyquist, Efficient computation of the two-dimensional periodic Green's function, *IEEE Tran. Antenna Propagat* **47** (May 1999), 895–897.

[20] K. Yasumoto, K. Yoshitomi and D.E. Goldgerg, *Genetic Algorithm in Search, Optimization and Machine Learning*, Addison-Wesley, 1989.

[21] E.C. Jordan and K.G. Balmain, *Electromagnetic Waves and Radiating Systems*, Englewood Cliffs, NJ: Prentice-Hall, 1968.

[22] S. Nakamura, *Applied Numerical Method in C*, Prentice-Hall int, 1993.